

Theory and applications of generalized Pipek–Mezey Wannier functions

Elvar Ö. Jónsson,¹ Susi Lehtola,^{1,2} Martti Puska,¹ and Hannes Jónsson^{1,3}

¹*COMP Centre of Excellence and Department of Applied Physics, Aalto University School of Science, P.O. Box 11100, FI-00076 Aalto, Espoo, Finland*

²*Chemical Sciences Division, Lawrence Berkeley National Laboratory, Berkeley, California 94720, United States^{a)}*

³*Faculty of Physical Sciences, University of Iceland, 107 Reykjavík, Iceland*

The theory for the generation of Wannier functions within the generalized Pipek–Mezey approach [Lehtola, S.; Jónsson, H. *J. Chem. Theory Comput.* **2014**, 10, 642] is presented and an implementation thereof is described. Results are shown for systems with periodicity in one, two and three dimensions as well as isolated molecules. The generalized Pipek–Mezey Wannier functions (PMWF) are highly localized orbitals consistent with chemical intuition where a distinction is maintained between σ - and π -orbitals. The PMWF method is compared with the so-called maximally localized Wannier functions (MLWF) that are frequently used for the analysis of condensed matter calculations. Whereas PMWFs maximize the localization criterion of Pipek and Mezey, MLWFs maximize that of Foster and Boys and have the disadvantage of mixing σ - and π -orbitals in many cases. The PMWF orbitals turn out to be as localized as the MLWF orbitals as evidenced by cross-comparison of the values of the PMWF and MLWF objective functions for the two types of orbitals. Our implementation in the atomic simulation environment (ASE) is compatible with various representations of the wave function, including real-space grids, plane waves and linear combinations of atomic orbitals. The projector augmented wave formalism for the representation of atomic core electrons is also supported. Results of calculations with the GPAW software are described here, but our implementation can also use output from other electronic structure software such as ABINIT, NWChem and VASP.

I. INTRODUCTION

Thanks to the continuing development of approximate density functionals in the past decades, Kohn–Sham density functional theory^{1,2} (KS-DFT) has become an essential workhorse of present-day computational chemistry and solid-state physics,³ allowing e.g. for the *in silico* design of new materials⁴. KS-DFT calculations are based on the variational minimization of an energy functional

$$E = E[n_\alpha, n_\beta] \quad (1)$$

that depends on the spin-up and spin-down electron densities n_α and n_β . In KS-DFT, the spin- σ density is represented by a fictitious system of non-interacting electrons as

$$n_\sigma(\mathbf{r}) = \sum_{i \text{ occ.}} |\phi_{i\sigma}(\mathbf{r})|^2, \quad (2)$$

which amounts to writing the wave function of the fictitious system as an antisymmetrized product i.e. a Slater determinant of non-interacting single-particle wave functions $\phi_{i\sigma}$ that are referred to as spin-orbitals. During the minimization of eq (1) with respect to the eq (2), the spin-orbitals are typically chosen to be the ones that diagonalize the effective one-particle Hamiltonian operator, because this leads to a decoupling of the differential equations for the optimal orbitals as²

$$\left[-\frac{1}{2}\nabla^2 + V(\mathbf{r}) + v_\sigma^{\text{xc}}(\mathbf{r}) \right] \phi_{i\sigma}(\mathbf{r}) = \epsilon_{i\sigma} \phi_{i\sigma}(\mathbf{r}). \quad (3)$$

Here, $V(\mathbf{r})$ is the external potential generated by the nuclei and the classical Coulomb potential generated by *all* the electrons, whereas v_σ^{xc} is the exchange-correlation potential which maps the fictitious non-interacting system onto the real, interacting system of electrons, which is not known in general but for which many approximations have been developed over the years³. The orbitals obtained from eq (3) are referred to as the *canonical orbitals* (COs), or *crystal(line) orbitals* in periodic systems.

As seen from eq (2), each electron in the system occupies some orbital and is seen to interact only with the average field generated by the nuclei and all the electrons in the system, since the energy functional, eq (1), only depends on the *total* spin densities $\{n_\sigma\}$. However, the COs typically extend over the whole system and *all* the orbitals therefore contribute to e.g. *any* covalent chemical bond between two atoms. But, the occupied orbitals in eqs (1) and (2) are arbitrary in the sense that any unitary transformation thereof, $\{\sum_{j \text{ occ.}} W_{ji}^\sigma \phi_{j\sigma}\}$, yields the same n_σ as $\{\phi_{i\sigma}\}$ if $(\mathbf{W}^\sigma)^\dagger = (\mathbf{W}^\sigma)^{-1}$. Once the COs have been determined, one can thus make a rotation of the occupied orbitals through some \mathbf{W}^σ that results in *localized orbitals* (LOs), which yield the same physical description of the system as the COs (as they span the same spin densities) but are confined to a smaller region of space. Because LOs can typically be interpreted in terms of chemical bonds, they can provide useful information about chemical interactions as well as a rationalization of the geometrical arrangement of atoms in molecules and solids⁵.

The same discussion as above for KS-DFT also applies to Hartree–Fock (HF) theory in that the HF orbitals are delocalized but the total energy is invariant under rotation of the occupied orbitals, and more meaningful LOs

^{a)}Electronic mail: susi.lehtola@alumni.helsinki.fi

can therefore be formed with post-processing of HF calculations. Unfortunately, there is no physical principle within KS-DFT or HF that would guide the choice of the LOs, so several different schemes have been suggested. The three that are most often used for isolated systems are the one proposed by Foster and Boys (FB), who suggested minimizing the second moment (i.e. variance) of the orbital densities⁶, the one proposed by Edmiston and Ruedenberg (ER), who suggested maximizing the self-Coulomb repulsion of the orbital densities⁷, and the one proposed by Pipek and Mezey (PM), who suggested maximizing Mulliken partial charge estimates⁸ per orbital on the atoms of the system⁹. Other schemes that have been suggested include the von Niessen (vN) scheme¹⁰, which maximizes the density self-overlap, the fourth moment (FM) scheme¹¹, which minimizes the fourth moment of the orbital spread (a variation on the FB scheme), and the natural bond orbital (NBO) method¹², which relies on the diagonalization of localized blocks of the one-electron density matrix. For the purpose of generating LOs, the various localization procedures usually produce similar results. However, one important advantage of the PM and NBO schemes over the others is that a proper separation of σ - and π -bond orbitals is maintained^{9,12}. The generation of LOs from HF orbitals (which are usually similar to KS-DFT orbitals) has been discussed recently by Høyvik and coworkers¹³.

While a multitude of localization methods exists for molecular systems, the available selection for solid state systems is more limited. In fact, it appears that the condensed matter community generally associates LOs in extended systems with the “maximally localized Wannier function” approach^{14,15}, which is an adaption of the original FB approach⁶ to periodic systems¹⁴. Non-iterative¹⁶ as well as iterative¹⁷ projection approaches for obtaining LOs in condensed matter calculations that are based on quasiatomic orbitals have also been presented in the literature, but they do not appear to have become widely used.

Here, it must be noted that the name “maximally localized Wannier functions” is rather unfortunate, because it implies that there is a unique, unambiguous way of determining the locality of orbitals. However, as discussed above and in ref. 15, orbital localization is not based on a single, rigorous, unifying physical principle. All of the localization methods listed above – the FB, ER, PM, vN, and FM approaches – rely on the optimization of some objective function, thus yielding maximally localized orbitals **as determined by that objective function**. Instead, “maximally localized Wannier functions” should rather be called Foster–Boys Wannier functions (FBWF), and we will use that convention throughout the rest of this article. Furthermore, as it has been shown recently that more localized *sets* of molecular orbitals than the ones reproduced by FB can be obtained by optimizing higher powers of the orbital spreads ($p > 1$, whereas FB uses $p = 1$), and/or by using the FM objective function instead of the FB one,¹¹ it is evident that more local-

ized Wannier functions than the ones produced by FBWF could be achieved.

A disadvantage of the FBWF approach is the mixing of σ and π orbitals. But, any scheme that can reproduce localized orbitals for molecules can also be used to produce Wannier functions¹⁸, i.e. LOs for a periodic system, in contrast to the Bloch states¹⁹ which constitute the extended COs. So, there is no reason why some of the other localization methods discussed above could not be adapted to periodic systems. While the ER, vN, and FM approaches tend to mix σ and π orbitals alike to the FB approach, the PM approach avoids such mixing and is often used for molecular systems. While PM has been used in Γ -point calculations of periodic systems based on localized basis sets and Mulliken analysis²⁰, a general formulation of the procedure for FD or PW based calculations has not been presented. Such a formulation can be problematic since Mulliken charges (and the related Löwdin charges) do not have a complete basis set limit.²¹

Modifications of the original PM scheme have, however, recently been presented by Lehtola and Jónsson in ref. 21, where the Mulliken partial charge estimate can be replaced by a variety of different, mathematically well-founded alternatives based on e.g. a real-space division of the system into atomic regions. The schemes studied in ref. 21 included the Voronoi (a.k.a. Wigner–Seitz in periodic systems) partitioning, Hirshfeld²² or iterative Stockholder partitioning^{23,24}, and Bader²⁵ partitioning, among others. It was shown in ref. 21 that similar mathematically better-defined modifications of the PM objective function had been proposed earlier in the literature. Cioslowski used a localization scheme based on Bader charges,²⁶ and Alcoba et al. later replaced them with “fuzzy atom” charges²⁷. Neither scheme has become widely used, which we attribute to the lack of the connection to the PM method that was established in ref. 21. Simultaneously to our work in ref. 21, another modification of the Pipek–Mezey method using charge estimates based on free-atom orbitals (“intrinsic atomic orbitals”, IAOs) was proposed by Knizia²⁸, who coined the resulting LOs as “intrinsic bond orbitals” (IBOs).

An important aspect of the results presented in ref. 21 is the realization that the orbitals obtained from a PM localization are remarkably insensitive to the choice of the partial charge estimate. Even qualitatively different estimates were found to yield similar LOs. Furthermore, for all choices of the partial charge estimate, a clear separation of σ - and π -bonds is maintained²¹. Since similar LOs can be obtained with a variety of dissimilar partial charge estimates, the original Pipek–Mezey method based on Mulliken charges as well as the schemes by Cioslowski, Alcoba et al. and Knizia can all be considered to be examples of a generalized PM method described in ref. 21.

Due to the robustness of the generalized PM method, there is significant flexibility in the choice of the partial charge estimate and this can be used to ensure that the

localization procedure is mathematically rigorous (thus guaranteeing well-defined basis set limits and robust convergence of the optimization) and also computationally convenient. By choosing the partial charges in the generalized PM scheme to be defined as integrals over the electron density in real-space, the approach can be ideally suited for condensed phase calculations.

Condensed matter simulations are typically based on a plane wave (PW) description of the electronic structure, while uniform real-space grids employing the finite difference (FD) approximation are becoming increasingly popular. Unlike the original procedure based on Mulliken charges that does not allow for straightforward application to PW or FD based calculations, the real-space choice for the partial charges does not depend on the use of an atom-localized basis set and thus can be readily implemented in PW or FD based calculations. Efficient grid-based approaches exist, for example, for the calculation of Bader charges²⁹. Improved partial charge estimation methods such as the iterative Hirshfeld method³⁰ have also been recently made available for condensed matter calculations³¹. However, due to the robustness of the generalized PM scheme, the use of such accurate partial charges is unnecessary as equally localized orbitals are obtainable with simpler charge estimates²¹.

In this article, we describe the theory and implementation of the generalized PM method for the formation of Wannier functions as a step to introduce this powerful approach for the chemical interpretation of electronic structure calculations to the toolbox of the condensed matter scientist. Our PMWF implementation supports both of the aforementioned, commonly used representations of the wave functions for solid state calculations – PWs and FD grids – as well as the linear combination of atomic orbitals (LCAO) approach. In addition, \mathbf{k} -point sampling is supported in our implementation. We find that the well-known superiority of the PM scheme to the FB scheme in the preservation of σ and π bonds is carried over to the Wannier functions: PMWFs turn out to be pure σ or π orbitals, while FBWFs in most cases have mixed σ and π character. Furthermore, PMWFs are found to be as localized as FBWFs in all of the systems studied.

The article is organized as follows. The generalized PM scheme of ref. 21 is briefly reviewed in the following Method section. Then, in the Implementation section, the specifics of extending the generalized PM scheme to the formation of Wannier functions are presented, and the two weight function schemes used in the present work (Hirshfeld and Wigner–Seitz partitioning) are described. In the Computational Details section, we describe how the calculations on various systems were performed, after which the calculated results for several systems are presented in the Results section. The article concludes with a Summary and Discussion section.

II. METHOD

The generalized PM method is briefly reviewed below. A more detailed account is given in ref. 21. The localization is done separately for the orbitals in each spin block, and in the following we will omit the spin indices. Localization is achieved by maximizing

$$\mathcal{P}(\mathbf{W}) = \sum_n^{N_{\text{occ}}} \sum_{\mathcal{A}=1}^{N_{\mathcal{A}}} [Q_{nn}^{\mathcal{A}}(\mathbf{W})]^p \quad (4)$$

where n sums over the N_{occ} occupied states, \mathcal{A} sums over all the $N_{\mathcal{A}}$ atoms in the system, p is a penalty exponent ($p = 2$ in the present work), and \mathbf{W} is a unitary matrix that connects the COs ϕ_S to the LOs ψ_n as

$$\psi_n(\mathbf{r}) = \sum_R W_{Rn} \phi_R(\mathbf{r}) \quad (5)$$

$$\phi_S(\mathbf{r}) = \sum_m W_{Sm}^* \psi_m(\mathbf{r}) \quad (6)$$

The gradient descent procedure used for the optimization of eq (4) with respect to \mathbf{W} has been described elsewhere^{21,32}. An analogous problem of optimizing complex-valued occupied-occupied rotations also arises within self-interaction corrected density functional theory calculations³³, for which another parametrization of the optimization problem, including optional stability analysis, has been presented in ref. 34. Instead of simultaneous global orbital rotations, the optimization could also be performed using 2×2 Jacobi rotations of orbital pairs^{7,9}. While this approach generally works well, it may converge onto different solutions including saddle points depending on the orbital ordering, thus we prefer the global approach mentioned above. This choice is furthermore justified by the use of periodic boundary conditions that necessitate the use of complex orbitals for $\mathbf{k} \neq \mathbf{0}$. We are not aware of previous discussions of complex Jacobi rotations. Note that it might also be possible to circumvent the need for orbital optimization in the localization: for instance, a non-iterative variant of the real-space PM methods discussed in ref. 21 has recently been suggested by Heßelman³⁵, the extension of which to the case of periodic boundary conditions could be studied in future work.

The quantity $Q_{mn}^{\mathcal{A}}$ that appears in eq (4) is the atomic partial charge matrix for atom \mathcal{A} in the LO basis, which has the properties

$$Q_{nn}^{\mathcal{A}} \geq 0, \quad (7)$$

$$\sum_{\mathcal{A}}^{N_{\mathcal{A}}} Q_{nn}^{\mathcal{A}} = 1, \quad (8)$$

eq (7) stating that $Q_{mn}^{\mathcal{A}}$ must represent a non-negative norm and eq (8) that the LOs are normalized. Then, the number of electrons localized on atom \mathcal{A} can be obtained

as

$$\sum_n^{N_{\text{occ}}} Q_{nn}^{\mathcal{A}} = N_{\text{el}}^{\mathcal{A}}, \quad (9)$$

by summing over the individual orbital contributions. The (total) partial charge $q^{\mathcal{A}}$ on atom \mathcal{A} can be calculated as

$$q^{\mathcal{A}} = Z^{\mathcal{A}} - N_{\text{el}}^{\mathcal{A}}, \quad (10)$$

where $Z^{\mathcal{A}}$ is the atomic number of atom \mathcal{A} ; if pseudopotentials are used, $Z^{\mathcal{A}}$ is the effective atomic number without the frozen core electrons.

While a variety of estimates for the atomic charges can be used,²¹ we focus here exclusively on real-space methods. The total electron density, $n(\mathbf{r})$, is partitioned in real-space into atomic densities through the atomic weight function $w_{\mathcal{A}}(\mathbf{r})$

$$n_{\mathcal{A}}(\mathbf{r}) = w_{\mathcal{A}}(\mathbf{r})n(\mathbf{r}). \quad (11)$$

The number of electrons on atom \mathcal{A} is then obtained as an integral

$$N_{\text{el}}^{\mathcal{A}} = \int n_{\mathcal{A}}(\mathbf{r})d^3r. \quad (12)$$

The necessary criteria for $w_{\mathcal{A}}$ are

$$0 \leq w_{\mathcal{A}}(\mathbf{r}) \leq 1 \quad (13)$$

and

$$\sum_{\mathcal{A}}^{N_{\mathcal{A}}} w_{\mathcal{A}}(\mathbf{r}) = 1, \quad (14)$$

which allow for a great deal of freedom when choosing the weight functions. In this formulation, $Q_{mn}^{\mathcal{A}}$ is obtained as

$$Q_{mn}^{\mathcal{A}} = \int \psi_m^*(\mathbf{r})w_{\mathcal{A}}(\mathbf{r})\psi_n(\mathbf{r})d^3r, \quad (15)$$

where ψ_m and ψ_n are LOs, and $w_{\mathcal{A}}(\mathbf{r})$ is a real-space weight function corresponding to atom \mathcal{A} . Again, since various weight functions for the generalized PM method have previously been found to give similar localized orbitals,²¹ we choose here simple and efficient methods for constructing the weight function, as described below in the Implementation section.

The reason why the generalized PM and PMWF methods do not mix σ and π bonds in planar systems lies in the orbital rotation gradient for orbitals i and j which is proportional to³² $Q_{ij}^{\mathcal{A}}$. The rotation gradient must vanish when the optimization objective function has been maximized. However, $Q_{\sigma\pi}^{\mathcal{A}} = 0$ for a real-space division of the molecule, assuming the the weight function is even under reflection over the molecular plane.²¹ Thus, even if the optimization is started from orbitals that have mixed

σ - π character, the orbital rotation gradient will end up separating these components into σ - and π -type orbitals. A similar discussion including stability analysis has been given in ref. 9 for the original Pipek–Mezey formulation using Mulliken charges.

The corresponding matrix elements in the FB optimization, however, do not possess similar symmetry properties and as a result FB (and FBWF) end up mixing σ and π orbitals. FBWF can be coaxed to reproduce σ - π separation if one allows mixing of occupied and unoccupied orbitals^{36,37}. However, the orbitals then become partially occupied instead of being fully occupied, or not occupied at all. Therefore, the interpretation of the results becomes more challenging, as a single electron may be simultaneously represented by multiple orbitals. As an extreme, if all valence unoccupied orbitals are included in such a procedure, the localization will just reproduce basis functions localized on the atoms and the resulting orbitals end up being devoid of chemical information about the system being studied. In contrast, the PM and PMWF approaches yield proper σ - π separation without needing to resort to partial occupation numbers, which makes e.g. the chemical interpretation and use in post-Hartree–Fock methods simpler.

Alternatively, when the global symmetry of the system allows for the *a priori* identification of σ and π states, localization procedures can be restricted to operate within the set of orbitals of a given symmetry. While this procedure enables any localization method to yield pure σ and π orbitals, the constraint of no mixing of σ and π states in the optimization also means that the resulting LOs may be less localized than what they would be without such constraints. An application of symmetry restrictions to FBWF has been presented recently³⁸. However, point group symmetries that allow for the *a priori* grouping of orbitals are only present in limited special cases. The PMWF approach presented here is a general purpose tool where special restrictions do not need to be introduced to obtain proper separation of σ and π orbitals.

III. IMPLEMENTATION

Because the maximization of eq (4) needs many evaluations of $Q_{mn}^{\mathcal{A}}$, a $N_{\text{occ}} \times N_{\text{occ}}$ matrix for every atom \mathcal{A} , it makes technically more sense to evaluate

$$\tilde{Q}_{RS}^{\mathcal{A}} = \int \phi_R^*(\mathbf{r})w_{\mathcal{A}}(\mathbf{r})\phi_S(\mathbf{r})d^3r, \quad (16)$$

where $\tilde{Q}^{\mathcal{A}}$ is the atomic partial charge matrix in the CO basis and ϕ_R and ϕ_S are occupied COs, to construct $Q_{mn}^{\mathcal{A}}$ as

$$Q_{mn}^{\mathcal{A}} = \sum_{RS} W_{Rm}^* \tilde{Q}_{RS}^{\mathcal{A}} W_{Sn} \quad (17)$$

where R and S index the occupied COs. This way, the expensive numerical integration in eq (16) needs to be

done only once at the beginning of the calculation, and the matrices may be stored on disk so that only the matrix corresponding to a given atom \mathcal{A} needs to be kept in memory at a time.

Moving on to a periodic system, the maximization of the objective function in eq (4) now includes periodic images through the overlap matrices which are defined in terms of³⁹ primitive lattice vectors $\{G_\alpha\}$ (three for orthorhombic cells as implemented here) with corresponding weights $\{g_\alpha\}$. The definitions of the vectors and weights can be found in refs. 20,40, which present a generalization of the overlap matrices for cubic periodic systems⁴¹ to any cell symmetry but restricted to the Γ -point. However, by defining a \mathbf{k} -point mesh³⁷ in terms of an artificially expanded unit-cell, the method is applicable to periodic systems with \mathbf{k} -point sampling. A brief overview of the lattice vector definitions is presented in the appendix.

For periodic systems the COs are represented in terms of Bloch functions

$$\phi_{S\mathbf{k}}(\mathbf{r}) = e^{i\mathbf{k}\cdot\mathbf{r}} u_{S\mathbf{k}}(\mathbf{r}) \quad (18)$$

where $u_{S\mathbf{k}}$ has the periodicity of the lattice. In analogy to eq (5), the n :th LO is given by

$$\psi_{n,c}(\mathbf{r}) = \frac{1}{\sqrt{N_{\mathbf{k}}}} \sum_{\mathbf{k}} \sum_S W_{S\mathbf{k}}^{\mathbf{k}} e^{-i\mathbf{k}\cdot\mathbf{R}_c} \phi_{S\mathbf{k}}(\mathbf{r}) \quad (19)$$

relative to unit cell c , where $N_{\mathbf{k}}$ is the number of \mathbf{k} -points and \mathbf{R}_c is any Bravais lattice vector. The objective function of eq (4) becomes

$$\mathcal{P}(\mathbf{W}) = \sum_n \sum_{\mathcal{A}} \sum_{\alpha}^{N_{\text{occ}}} g_\alpha |Q_{\alpha,nn}^{\mathcal{A}}(\mathbf{W})|^p, \quad (20)$$

where $\tilde{Q}^{\mathcal{A}}$ and \mathbf{W} now take on a \mathbf{k} -dependent form

$$Q_{\alpha,mn}^{\mathcal{A}} = \sum_{\mathbf{k}\mathbf{k}'} \sum_{RS} (W_{Rm}^{\mathbf{k}})^* \tilde{Q}_{\alpha,RS}^{\mathcal{A},\mathbf{k}\mathbf{k}'} W_{Sn}^{\mathbf{k}'}. \quad (21)$$

Eq (16) can be written as³⁹

$$\tilde{Q}_{\alpha,RS}^{\mathcal{A},\mathbf{k}\mathbf{k}'} = \int u_{R\mathbf{k}}^*(\mathbf{r}) w^{\mathcal{A}}(\mathbf{r}) u_{S\mathbf{k}'}(\mathbf{r}) e^{i(\mathbf{k}'-\mathbf{k}-\mathbf{G}_\alpha)\cdot\mathbf{r}} d^3r \quad (22)$$

which is nonzero only when $\mathbf{k}' = \mathbf{k} + \mathbf{G}_\alpha$. This reduces the double sum over \mathbf{k} and \mathbf{k}' in eq (21) to a single sum over \mathbf{k} . However, the optimization of the unitary rotation matrices at the \mathbf{k} -points, $\{\mathbf{W}^{\mathbf{k}}\}$, depends on neighbouring \mathbf{k} -points as well ($\mathbf{k}' = \mathbf{k} + \mathbf{G}_\alpha$).

As in typical implementations⁴² of its parent method – the FB approach⁶ – the objective function optimized in practical implementations of the FBWF method^{14,15,36,37,43} is not based on the minimization of the orbital spread, but on the equivalent task of maximizing the sum of squares of distances of orbital centroids from the origin of the coordinate system^{39,40}

$$\mathcal{L}(\mathbf{W}) = \sum_n \sum_{\alpha}^{N_{\text{occ}}} g_\alpha |Z_{nn}^{\alpha}|^2 \quad (23)$$

where

$$Z_{nn}^{\alpha} = \sum_{RS} W_{Rn}^* Z_{SR}^{\alpha} W_{Sn} \quad (24)$$

and

$$Z_{SR}^{\alpha} = \langle \phi_R^* | e^{-i\mathbf{G}_\alpha\cdot\mathbf{r}} | \phi_S \rangle, \quad (25)$$

and a similar unitary optimization problem is solved as in the PMWF method.

The task of maximizing the objective function of eq (20), when restricted to $p = 2$, is similar to the task of maximizing eq (23), so methods used to maximize eq (23) – employing, for example, steepest descent algorithms^{37,41} – are applicable to eq (20). This means that existing FBWF codes based on maximizing the objective function of the eq (23) form could easily be modified to generate PMWFs instead.

A. Weight functions

Two different forms of the weight function were chosen for the present work: a Gaussian weight function, which results in a fuzzy real-space partitioning of the system into atomic regions, and Wigner–Seitz partitioning, which divides the system into non-overlapping atomic regions. In agreement with the results of ref. 21, these two qualitatively different weight functions are found to produce similar LOs despite predicting strikingly different atomic partial charges, as will be seen in the Results section.

B. Gaussian weight

A simple choice of the weight function (eqs (13) and (14)) is obtained using a Hirshfeld-type²² partitioning

$$w_{\mathcal{A}}(\mathbf{r}) = \frac{\bar{n}_{\mathcal{A}}(\mathbf{r})}{\sum_{\mathcal{A}'=1}^{N_{\mathcal{A}}} \bar{n}_{\mathcal{A}'}(\mathbf{r})} \quad (26)$$

where $\bar{n}_{\mathcal{A}}$ are spherically symmetric functions that could be gas-phase atom densities (as in the original Hirshfeld scheme), or iteratively defined atom densities such as in the iterative Hirshfeld^{30,44,45} or the iterative Stockholder schemes^{23,24}. Based on the experience from ref. 21 that the generalized PM scheme is insensitive to the partial charge estimate, we choose simple Gaussian model densities

$$\bar{n}_{\mathcal{A}}(\mathbf{r}) = \frac{N_{\text{el},\mathcal{A}}}{\gamma_{\mathcal{A}} \sqrt{2\pi}} \exp \left\{ -\frac{(\mathbf{r} - \mathbf{R}^{\mathcal{A}})^2}{2\gamma_{\mathcal{A}}^2} \right\} \quad (27)$$

where $N_{\text{el},\mathcal{A}}$ is the (effective) number of electrons on atom \mathcal{A} and $\mathbf{R}^{\mathcal{A}}$ is its position. This model was used by Oberhofer and Blumberger⁴⁶ in the context of constrained

density functional theory. They found that qualitatively similar results were obtained when using spherical neutral free atom densities and the Gaussian model densities. Furthermore, the charge constrained energy did not depend strongly on the choice of decay parameter $\gamma_{\mathcal{A}}$ in the range $\gamma_{\mathcal{A}} \in [0.5 \text{ \AA}, 1.0 \text{ \AA}]$.

Results presented here using the Gaussian model densities were obtained with a decay parameter value of $\gamma_{\mathcal{A}} = 0.5 \text{ \AA}$ for all types of atoms, unless stated otherwise. A different choice for the decay parameter results in practically the same localized orbitals, but with different total partial atomic charges (eq (9)). The form of eq (27) is convenient as the fast decay of the model density allows for efficient spatial screening of contributions.

C. Wigner–Seitz partitioning

Alternatively, the weight function can be based on non-overlapping atomic regions defined using, for example the Bader²⁵ or the Wigner–Seitz schemes, for which the weight function is a step function

$$w_{\mathcal{A}}(\mathbf{r}) = \begin{cases} 1 & \text{if } \mathbf{r} \in \mathcal{A} \\ 0 & \text{otherwise} \end{cases} \quad (28)$$

that clearly satisfies the criteria of eqs (13) and (14). The Wigner–Seitz scheme corresponds to the Voronoi scheme discussed in ref. 21 since Wigner–Seitz cells are Voronoi cells. The Wigner–Seitz scheme is parameter-free, easy to construct on a grid, and forms the second class of weight functions chosen for the present work. Furthermore, this scheme is even more convenient than the Gaussian weights for use with periodic systems, since it has a clear cut-off in any dimension which is particularly convenient when periodicity is present.

IV. COMPUTATIONAL DETAILS

The electronic structure calculations in this work are performed with the GPAW program⁴⁷. There, the wave functions can be represented using any of the three aforementioned approaches: with real-space grids, atomic orbitals⁴⁸, or plane waves, and any of these representations can be used in the present PMWF implementation. The present results have been obtained using the FD approach, unless otherwise stated. We also present a few cases where the PW and LCAO approaches have been used.

All the electronic structure calculations in this work made use of the PBE⁴⁹ exchange-correlation functional, using a 360 eV kinetic energy cutoff for PWs, a 0.18 \AA spacing for FD, and the "dzp"-basis for the LCAO. A convergence criterion of 0.05 eV/ \AA was used for the forces to relax the nuclear degrees of freedom. Core electrons were described with the projector augmented wave (PAW) method⁵⁰. Periodic boundary conditions

employed a Monkhorst–Pack grid⁵¹ to sample the Brillouin zone with dimensions of (3,1,1), (3,3,1) and (3,3,3) for the systems with periodicity in one, two, and three dimensions, respectively. The unit cell dimension was relaxed along the directions on which periodic boundary conditions were applied, whereas a 7 \AA vacuum region was included on both sides of the system along non-periodic directions.

The PMWF method has been implemented as a standalone object-oriented package in the Atomic Simulation Environment⁵² (ASE) library. The implementation supports the use of PAW for the core electrons; the PAW specific details of the implementation are given in the Appendix. While our results were obtained with GPAW, the implementation in ASE can also be used with other software packages for which ASE has an interface, such as ABINIT⁵³, NWCHEM⁵⁴, and VASP⁵⁵.

All surfaces are drawn with the open-source software package Jmol⁵⁶, at an isosurface value corresponding to a 75% density cut-off as described in the appendix of ref. 21. In contrast to the common approach of using a fixed isosurface value for all orbitals, the density isosurfaces constitute an unambiguous visualization method, as the value of the isosurface will reflect how localized an orbital is. This way all orbitals are treated on equal footing, regardless of their character.

A. Analysis of localized states

To analyze the σ - or π -bond mixing of the PMWFs and FBWFs, the COs are first classified into σ and π states. This operation is trivial for linear and planar systems, as the mirror symmetry operator (\mathcal{M}) through the molecular or periodic plane leaves σ states unchanged whereas π states undergo a phase change; that is

$$\mathcal{M}\sigma(x, y, z) \equiv \sigma(x, y, -z) = \sigma(x, y, z) \quad (29)$$

$$\mathcal{M}\pi(x, y, z) \equiv \pi(x, y, -z) = -\pi(x, y, z) \quad (30)$$

The σ - and π -bond mixing of the PMWFs and FBWFs can then easily be calculated, since the expansion coefficients of the n :th PMWF or FBWF in terms of the COs are the n :th rows of the optimized unitary matrix (eq (19)). The fractions of σ and π type character in the n :th LO, f_n^σ and f_n^π , respectively, can be obtained as

$$f_n^\sigma = \sum_{\sigma\text{-type } S} W_{S_n}^* W_{S_n} \quad (31)$$

$$f_n^\pi = \sum_{\pi\text{-type } S} W_{S_n}^* W_{S_n} \quad (32)$$

Because there is no unique way of defining orbital locality, the values of the PMWF and FBWF objective functions, eqs (20) and (23), are used as measures of localization for both PMWF and FBWF orbitals. The FBWF measures are computed with the pre-existing implementation in ASE (see ref. 37), and the PMWF measures are obtained with the method described here.

TABLE I: Value of the objective function, eq (20), and atomic charge estimates, eq (10), for cis-polyacetylene (see main text).

basis	$\mathcal{P}(\mathbf{W})$	$Q_C / -Q_H$
LCAO	8.74	0.058
FD	8.71	0.062
PW	8.70	0.065

V. RESULTS

A variety of systems were calculated with KS-DFT as described above in the Computational Details section, and the resulting COs localized using both the FBWF and PMWF approaches. COs and LOs for various systems are shown in figures 1 to 5. In some cases the PMWF and FBWF methods give qualitatively similar results and the visual comparison is, hence, omitted, but the results are noted in the main text. The systems studied range from isolated molecules (benzene, coronene, supercoronene), to systems with one- (polyethylene, polyacetylene, carbyne, armchair nanoribbons), two- (graphene, boron nitride) or three-dimensional (benzene crystal) periodicity.

A. Comparison of basis and partitioning functions

Unlike the mathematically ill-founded Mulliken charges that were used in the original Pipek–Mezey scheme⁹, the generalized Pipek–Mezey schemes²¹ of refs. 21,26–28 rely on mathematically well-defined partial charge estimates that provide smooth convergence to the basis set limit. Table I presents the generalized Pipek–Mezey objective function values and atomic charge estimates for cis-polyacetylene, where the COs are described with the FD, PW, or LCAO bases in GPAW. A convergence test in the FD and PW bases reveals that the value of the objective function (eq (20)) and the partial atomic charges (eq (10)) reach constant values at a grid-spacing of 0.3 Å or a kinetic energy cut-off of 300 eV, for the two bases, respectively. These are well within the typical range of values used for FD and PW calculations, and should not pose problems for typical applications.

In the PMWF method the atomic partial charge matrix, eq (16), depends on the choice of the atomic weight function. This dependence suggests that the orbitals that maximize the PMWF objective function could also depend on the weight function used. However, in ref. 21 the orbitals were found by visual comparison to be remarkably insensitive to the choice of the partial charge estimate, even while the resulting atomic (total) partial charge assignment varied greatly. We confirm this result for the partitioning functions used in the present work – the Hirshfeld-type weight function using Gaussian model densities (eqs (26) and (27), respectively) with various

TABLE II: Atomic charge estimates, eq (10), in a boron nitride sheet using Wigner–Seitz (WS) and Hirshfeld (H) function definition of partial charges with three different choices for the decay parameter of the boron atoms, γ_B (see main text).

$w_A(\mathbf{r})$	$Q_B / -Q_N$
WS	0.369
H, $\gamma_B = 0.50$ Å	0.490
H, $\gamma_B = 0.75$ Å	-0.224
H, $\gamma_B = 1.00$ Å	-0.651

choices for the atomic decay parameters, as well as the Wigner–Seitz weight function (eq (28)).

The number of electrons localized on the atoms (eq (12)) in a periodic boron nitride sheet was estimated with the two choices of weight functions: The Wigner–Seitz (WS) function (eq (28)), and the Hirshfeld-type (H) function (eq (26)). Different choices for the decay parameter in the Gaussian model density (eq (27)) for boron γ_B were considered, while the decay parameter for nitrogen is kept fixed at $\gamma_N = 0.5$ Å. Table II presents the resulting atomic charge estimates (eq (9)), where the partial charge on the nitrogen atoms is the negative of that on the boron atoms. The Wigner–Seitz and Hirshfeld function with symmetric decay factors describe boron as a donor, while increasing the value of the decay parameter of boron (thus ascribing more space – and electrons – to it) makes it an acceptor in the partial charge analysis.

While the partial charges on the atoms estimated by the various models are clearly different – showing a variation larger than one elementary charge unit – they all result in nearly identical LOs, and no discernible difference can be seen for the 75% density²¹ isosurfaces. For this reason, only the PMWFs for the Wigner–Seitz weight scheme are shown in figure 1. This is in agreement with the result found for molecules in ref. 21, highlighting the versatility of the PM method in achieving orbital localization even with partial charge estimates that disagree with chemical intuition – as long as the charge estimates are mathematically well-defined²¹.

To quantify the similarity of the PMWF orbitals obtained with the different choices of the atomic charge definitions, their overlap was evaluated. For two sets of PMWFs, $\{\psi_n^A\}$ and $\{\psi_n^B\}$, obtained from the use of two different weight functions w^A and w^B in the localization procedure, the residual overlap matrix is evaluated

$$R_{mn}^{AB} = |\langle \psi_m^A | \psi_n^B \rangle|^2 - \delta_{mn}, \quad (33)$$

in analogy to what was recently used to analyze the orbital convergence of self-interaction corrected density functional theory calculations³⁴. The ordering and complex phases of the orbitals for two identical calculations started from a different random starting point may differ³⁴ (e.g. $|\psi_n\rangle$ spans the same orbital density as $|\psi_n^*\rangle$ while their overlaps differ), but we circumvent both of

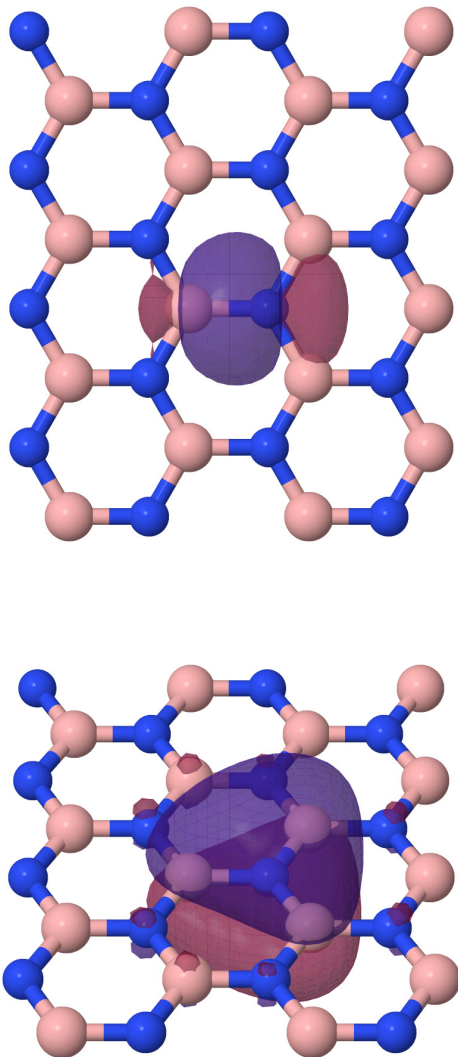


FIG. 1: Pipek–Mezey orbitals in boron nitride, represented by $B_{16}N_{16}$ sheet in a two-dimensional periodic lattice, obtained with the Wigner–Seitz weight function (see main text).

these problems by carrying out one optimization for the PMWFs with one choice for the weight function – the Hirshfeld function with symmetric decay factors – and then by using the orbitals from this calculation as starting guesses for the other choices of the weight function.

The diagonal of \mathbf{R}^{AB} measures the similarity of the localized orbitals produced using weight schemes A and B. Thus, the similarity is quantified by

$$R_{\max}^{AB} = \max_n R_{nn}^{AB}, \quad (34)$$

$$R_{\text{rms}}^{AB} = \sqrt{\sum_{n=1}^N (R_{nn}^{AB})^2 / N}, \quad (35)$$

that is, the maximum and root-mean-square (rms) deviations, respectively, from perfect insensitivity to the used

weight metric. The results are shown in table III, from which the degree of similarity is apparent. The overlaps are close to unity, once again confirming the robustness of the generalized Pipek–Mezey scheme. In the rest of the calculations presented here, the Hirshfeld-type weighting factor was used with equal-valued decay factors.

B. Localized states and σ - and π -bond mixing

The mixing of σ - and π -bond orbitals is analyzed by calculating the σ and π projections of the PMWFs and FBWFs using eqs (31) and (32), respectively. This analysis is performed for all planar systems, carbyne, and cis-polyacetylene, and the results are presented in table IV. Localized states in the set of PMWFs and FBWFs which are not mixed and clearly represent σ - and π -bonds are denoted $\sigma_{AA'}$ and $\pi_{AA'}$, respectively. Mixed σ and π states are denoted τ , following ref. 9. It is clear from table IV that the mixing of σ - and π -bond orbitals in the FBWF method occurs systematically for the aromatic hydrocarbons. In aromatic systems a π -bond orbital exists for every two carbon atoms. The consistent 50/50 mixing of σ and π states doubles the number of π -type orbitals in the FBWF set, and as a result reduces the number of σ_{CC} -bond orbitals. No pure π -bond orbitals are found, and a τ mixed state (“banana” shaped orbitals, as coined by Pipek and Mezey⁹) exists for every carbon atom, resulting in a distorted chemical picture for this type of system. The set of PMWFs contain a localized σ_{CC} for each possible carbon-carbon bond, and a π_{CC} for every two carbon atoms – there is no mixing found between the σ and π states – representing the conventional chemical picture of the aromatic hydrocarbons. Both sets represent all possible σ_{CH} -bonds with similar degree of localization.

For the aromatic hydrocarbons – benzene, coronene, supercoronene and armchair nanoribbons – both the PMWF and FBWF methods reduce the set of COs, which are distinct for each valence state, to a set of a few highly localized orbitals representing the σ - and π -bonds. Figure 2 presents example COs and LOs for a (2,4)-armchair nanoribbon. The Kohn–Sham states spread over the entire system. For the FBWF and PMWF methods, the first and second column show example σ -bond orbitals, which are highly localized carbon-hydrogen (σ_{CH})- and carbon-carbon (σ_{CC})-bonds, whereas the third and fourth columns show examples of states with π character, which are pure π states for PMWF but mixtures of σ - and π -bond orbitals in the case of FBWF.

COs, FBWFs and PMWFs for cis-polyacetylene are presented in figure 3. The FBWF and PMWF methods give similar orbitals corresponding to σ_{CC} (first column) and σ_{CH} bonds (middle column), but the FBWFs do not appear as localized as the PMWFs as judged by the 75% density isosurfaces. Only four σ_{CC} bonds of the eight possible σ_{CC} -bonds in the system are obtained with the FBWF method, while the other four are mixed with the

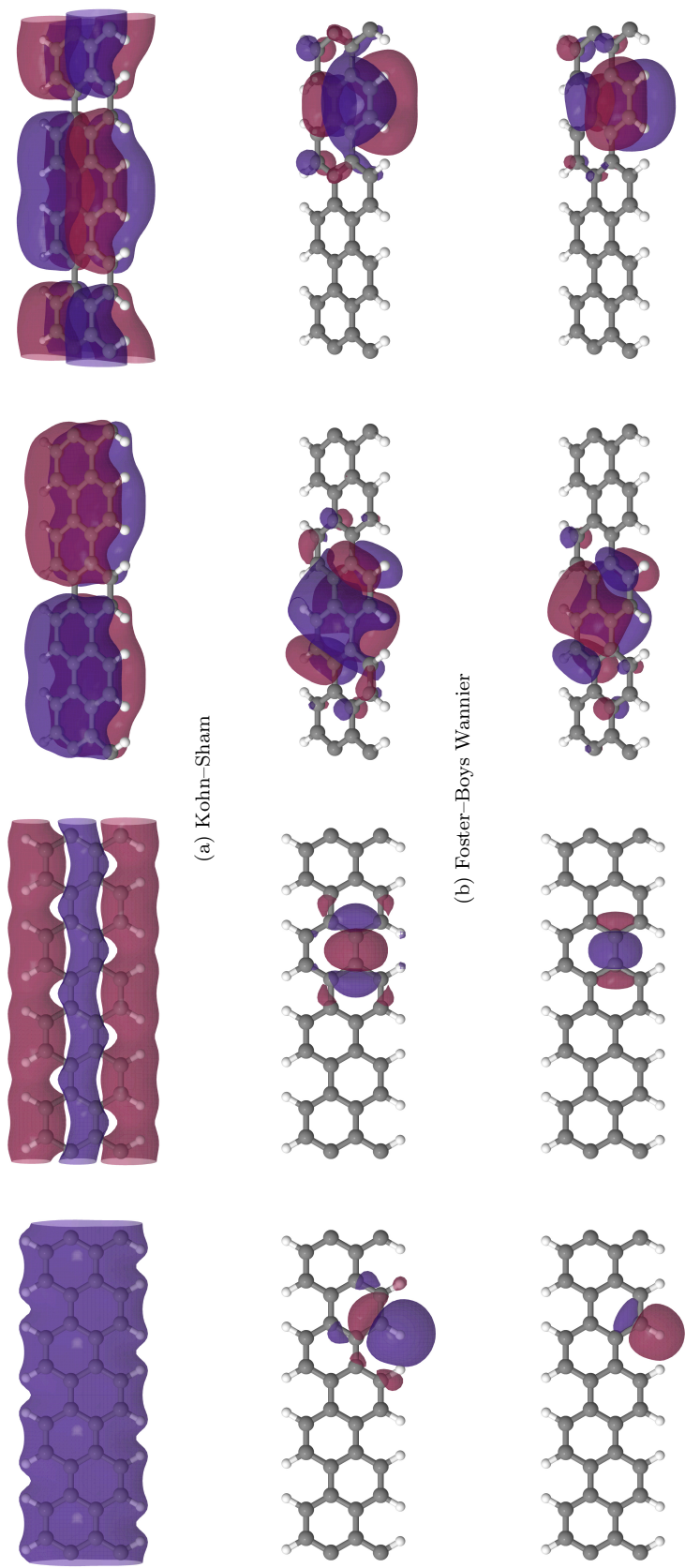


FIG. 2: Kohn-Sham (top row), Foster-Boys Wannier function (middle row) and Pipek-Mezey Wannier function (bottom row) orbitals of (2,4)-armchair nanoribbon segment, subject to periodic boundary conditions (see main text).

TABLE III: Analysis of the similarity of PMWFs obtained using various atomic weighing schemes. The first row and first column indicate A and B in eq (33). The lower triangle gives $\lg(R_{\text{rms}})$ (eq (35)) and the upper triangle gives $\lg(R_{\text{max}})$ (eq (34)).

$w_{\mathcal{A}}(\mathbf{r})$	WS	H, $\gamma_B = 0.50 \text{ \AA}$	H, $\gamma_B = 0.75 \text{ \AA}$	H, $\gamma_B = 1.00 \text{ \AA}$
WS		-3.1	-3.1	-3.0
H, $\gamma_B = 0.50 \text{ \AA}$	-3.3		-3.7	-3.2
H, $\gamma_B = 0.75 \text{ \AA}$	-3.3	-3.8		-3.7
H, $\gamma_B = 1.00 \text{ \AA}$	-3.2	-3.4	-4.2	

TABLE IV: Number of σ , π and τ bonding states in the set of PMWFs and FBWFs, as well the expansion of the τ states in σ and π type COs (see main text).

System	PMWFs	FBWFs	τ composition
benzene	$6\sigma_{\text{CC}}, 6\sigma_{\text{CH}}, 3\pi_{\text{CC}}$	$3\sigma_{\text{CC}}, 6\sigma_{\text{CH}}, 6\tau$	$50\%\sigma + 50\%\pi$
coronene	$30\sigma_{\text{CC}}, 12\sigma_{\text{CH}}, 12\pi_{\text{CC}}$	$18\sigma_{\text{CC}}, 12\sigma_{\text{CH}}, 24\tau$	$50\%\sigma + 50\%\pi$
supercoronene	$72\sigma_{\text{CC}}, 18\sigma_{\text{CH}}, 27\pi_{\text{CC}}$	$45\sigma_{\text{CC}}, 18\sigma_{\text{CH}}, 54\tau$	$50\%\sigma + 50\%\pi$
AC(2,4)	$40\sigma_{\text{CC}}, 16\sigma_{\text{CH}}, 16\pi_{\text{CC}}$	$24\sigma_{\text{CC}}, 16\sigma_{\text{CH}}, 32\tau$	$50\%\sigma + 50\%\pi$
AC(3,3)	$48\sigma_{\text{CC}}, 12\sigma_{\text{CH}}, 18\pi_{\text{CC}}$	$30\sigma_{\text{CC}}, 12\sigma_{\text{CH}}, 36\tau$	$50\%\sigma + 50\%\pi$
AC(4,3)	$66\sigma_{\text{CC}}, 12\sigma_{\text{CH}}, 24\pi_{\text{CC}}$	$42\sigma_{\text{CC}}, 12\sigma_{\text{CH}}, 48\tau$	$50\%\sigma + 50\%\pi$
benzene crystal	$24\sigma_{\text{CC}}, 24\sigma_{\text{CH}}, 12\pi_{\text{CC}}$	$12\sigma_{\text{CC}}, 24\sigma_{\text{CH}}, 34\tau$	$50\%\sigma + 50\%\pi$
cis-polyacetylene	$8\sigma_{\text{CC}}, 8\sigma_{\text{CH}}, 4\pi_{\text{CC}}$	$4\sigma_{\text{CC}}, 8\sigma_{\text{CH}}, 8\tau$	$50\%\sigma + 50\%\pi$
carbyne	$8\sigma_{\text{CC}}, 8\pi_{\text{CC}}$	$4\sigma_{\text{CC}}, 12\tau$	$33\%\sigma + 66\%\pi$
graphene	$48\sigma_{\text{CC}}, 16\pi_{\text{CC}}$	$48\sigma_{\text{CC}}, 16\pi_{\text{CC}}$	
boron nitride	$48\sigma_{\text{BN}}, 16\pi_{\text{BN}}$	$48\tau^A, 16\tau^B$	$\tau^A : 97\%\sigma + 3\%\pi$ $\tau^B : 9\%\sigma + 91\%\pi$

π_{CC} -bonds to form τ states as shown in the third column. The PMWF set consists of eight σ_{CC} -, eight σ_{CH} - and four π_{CC} -bonds, in accordance with the chemical picture of such a segment of cis-polyacetylene.

Figure 4 presents COs, FBWFs and PMWFs for carbyne. Here, there are in total 16 COs, half of them of σ character and the other half of π character. The FBWFs reduce to a set of two distinct types of orbitals, one representing the σ_{CC} -bond (first column) and the other being a set of τ mixed states (second column) that are a 33/66 mixture of σ and π COs. This composition arises because there are two π -bonds for every two carbon atoms, as carbyne has alternating single and triple bonds. Due to this mixing, only four of eight possible σ_{CC} bonds are represented by the set of FBWFs, with the other four being mixed with the π -bond orbitals to form twelve mixed τ -bond orbitals. In contrast, the set of PMWFs consists of eight σ_{CC} and eight π_{CC} bond orbitals, describing all possible carbon-carbon single and alternating triple bonds, matching the chemical picture of the carbyne segment.

The assignment of σ - and π -bond character for the COs is not as straightforward in the case of the benzene crystal (figure 5), as there is no global plane of symmetry. However, the resulting localized states associated with each molecule in the crystal should conform to eqs (29) and (30), unless they are a local mixture of σ and π . Indeed, a projection of the PMWFs about the molecular

planes reveals that proper σ - π separation is maintained. Just as for an isolated benzene molecule, each possible σ_{CC} -, σ_{CH} - and π_{CC} -bond in the crystal is described with highly localized states. In contrast, the set of FBWFs consists once again of twice the number of states with partial π character, and half the number of σ_{CC} states, compared to the COs, confirming that the same mixing applies here as in the case of the other aromatic hydrocarbons and cis-polyacetylene. Both methods produce similar σ_{CH} -bond orbitals (six in total), accounting for all possible carbon-hydrogen bonds, in line with earlier experience with the FB and PM methods^{21,32}.

In all the cases discussed above, a clear qualitative difference exists between the sets of PMWFs and FBWFs, with the latter method consistently mixing σ - and π -bond orbitals in systems with alternating single and double, or single and triple bonds.

For a periodic chain of polyethyl ($-\text{[C}_8\text{H}_{16}\text{]-}$), and a sheet of graphene (not depicted), the resulting FBWFs and PMWFs were found to be nearly identical in each case, although the FBWFs were found to be more diffuse as judged by the isosurface for which the integral of the orbital density²¹ reaches a value of 0.75. Contrary to the aromatic hydrocarbons and cis-polyacetylene, no mixing of σ and π states was found in the case of graphene in the set of FBWFs. A highly localized σ -bond exists for each possible atom pair in both LO sets, and a localized π -bond for every two carbon atoms in graphene. Unlike

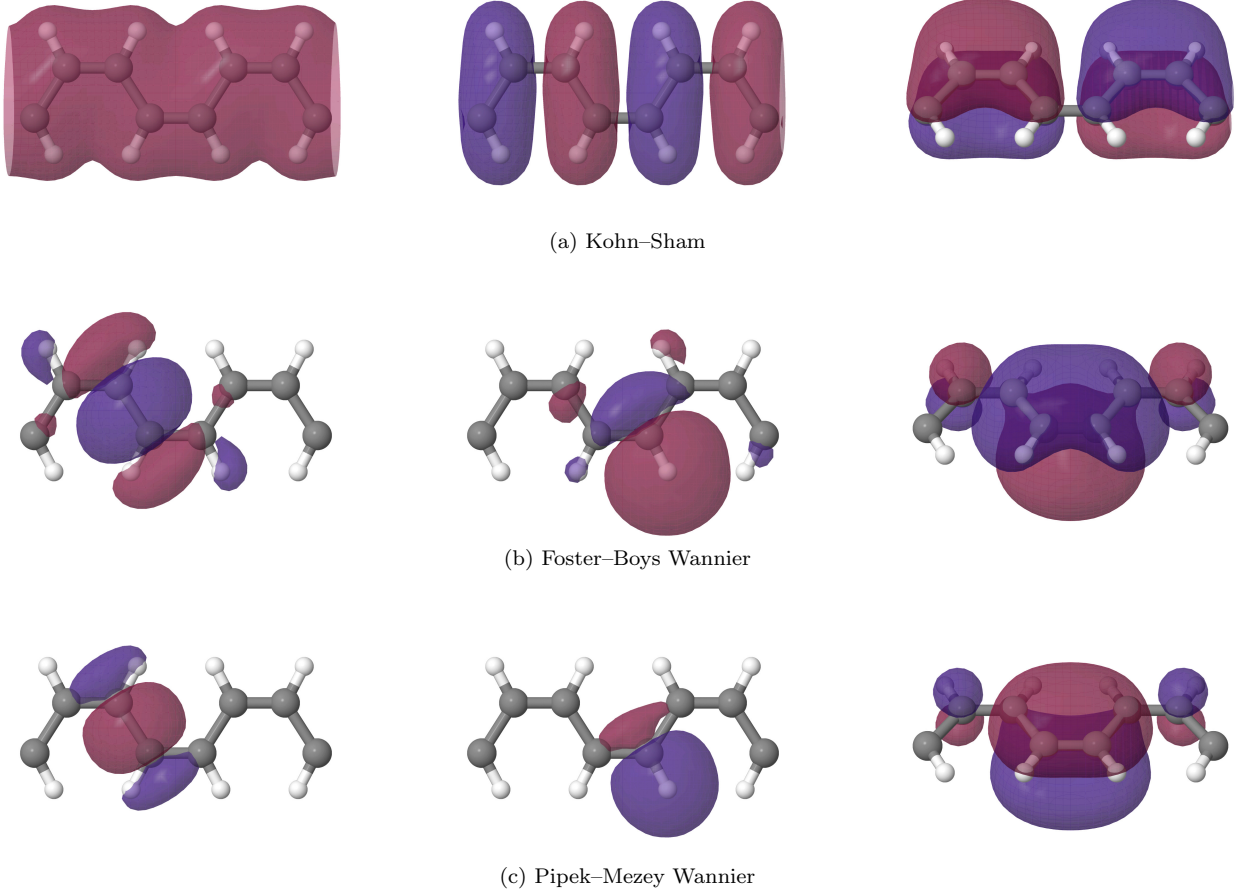


FIG. 3: Kohn-Sham (top row), Foster-Boys Wannier function (middle row) and Pipek-Mezey Wannier function (bottom row) orbitals of cis-polyacetylene, represented by a $-\text{[C}_8\text{H}_8\text{]}-$ segment, subject to periodic boundary conditions (see main text).

in graphene, the FBWFs in a sheet of boron nitride were found to consist of a slight mix of σ - and π -bond COs.

C. Localization measure of Pipek-Mezey orbitals

To measure the localization of the orbitals obtained using the PMWF method, we compare the values of the FBWF objective function \mathcal{L} (eq (23)) for COs, PMWFs, and FBWFs for all systems studied here in table V. While FBWFs systematically yield the largest values of this objective function (for which they have been optimized) – indicating the largest degree of locality – the values obtained for the PMWFs are very close: the difference

$$d = \frac{\mathcal{L}(\mathbf{W}^{\text{PMWF}}) - \mathcal{L}(\mathbf{W}^{\text{FBWF}})}{\mathcal{L}(\mathbf{W}^{\text{FBWF}})} \quad (36)$$

is well under 1% in every case. Relative to the localization measure for the COs, this difference is even less significant, meaning that as far as localization goes, the PMWF orbitals are practically as spatially localized as the FBWF orbitals, as judged by the FBWF criterion.

Similarly, the charge localization as measured by the PMWF objective function \mathcal{P} (eq (20)) is compared for COs, PMWFs, and FBWFs, and the differences between PMWFs and FBWFs are calculated by eq (36) by reversing the roles of the orbitals, as now PMWFs are by definition the most localized ones. The results are presented in table VI. PMWFs yield the largest values, indicating the largest degree of charge localization. However, the values obtained using FBWFs are very close to the optimal values given by the PMWFs, which states that FBWFs are practically as localized as PMWFs, as judged by the PMWF criterion. Thus, from the results in tables V and VI and the lack of a unique definition for orbital locality we can conclude that PMWFs are just as localized as FBWFs, which is one of the main results of this article.

In cases where σ - π mixing is not an issue and the FBWF and PMWF approaches give similar LOs, one might consider the FBWF method superior to the PMWF approach due to its greater computational efficiency: The evaluation of the FBWF cost function (eq (23)) requires the formation of one $N \times N$ matrix, N

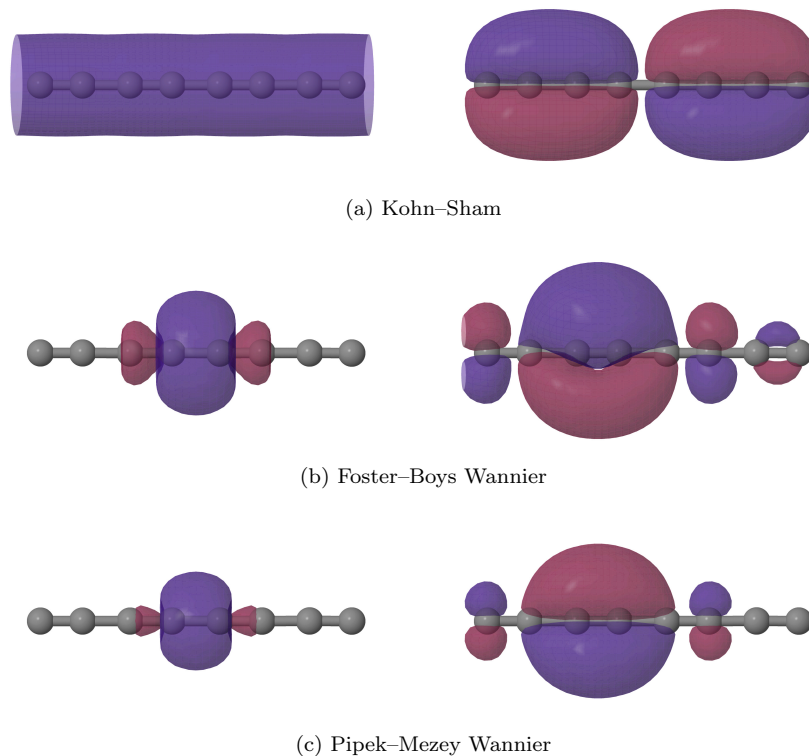


FIG. 4: Kohn-Sham (top row), Foster-Boys Wannier function (middle row) and Pipek-Mezey Wannier function (bottom row) orbitals of carbyne, represented by a $-[\text{C}_8]-$ segment subject to periodic boundary conditions (see main text).

being the number of occupied orbitals, whereas the evaluation of the PMWF cost function (eq (4)) requires the formation of $N_{\mathcal{A}}$ atomic $N \times N$ partial charge matrices. However, in our experience³² the optimization of PM LOs converges faster than that of FB LOs, and the larger cost of performing each step in PM optimization compared to FB may be compensated by the fewer number of iterations needed to optimize the PM cost function. Indeed, we have found this to be true also in the case of Wannier functions. Table VII reports the number of iterations $n_{\text{iter}}^{\text{PMWF}}$ and $n_{\text{iter}}^{\text{FBWF}}$ required to converge the PMWF and FBWF objective functions, respectively. The numbers in table VII have been averaged over fifty separate optimization runs with randomly initialized guesses for the localization matrix \mathbf{W} . The same minimization method is used for both objective functions³⁷. As can be seen from table VII, PMWF optimization typically requires up to an order of magnitude fewer iterations to converge.

There are also ways in which PMWF could be made faster: for large systems it’s possible to reformulate the localization problem in terms of some initial set of localized orbitals instead of the extended COs, as this will make \tilde{Q}_{RS}^A sparse. This initial set of orbitals could be obtained e.g. via the Cholesky decomposition of the density matrix⁵⁷. Approaches for the lossy compression of \tilde{Q}_{RS}^A could be pursued as well. However, because the postprocessing to obtain LOs is typically an insignificant

portion of runtime compared to the actual KS-DFT calculation to solve for the COs, we do not consider the potentially larger computational effort for PMWF compared to FBWF to be an issue.

VI. SUMMARY AND DISCUSSION

An extension of the generalized Pipek-Mezey method of ref. 21 for the formation of Wannier functions with the projector augmented wave formalism has been presented, as well as an implementation that supports \mathbf{k} -point sampling and multiple possible representations for the electronic wave function: plane waves, real-space grids, and linear combination of atomic orbitals. Applications of the method to a variety of different systems have also been presented, ranging from isolated molecules to periodic systems in one, two, and three dimensions. The Pipek-Mezey Wannier functions (PMWFs) have been compared to the commonly used “maximally localized Wannier functions”. However, since there is no unique, unambiguous way of defining the locality of orbitals and several possible measures for orbital locality have been defined in the literature (the orbitals corresponding to a given objective function are maximally localized *as determined by that objective function*), we choose to refer to Foster-Boys Wannier functions (FBWFs) instead of

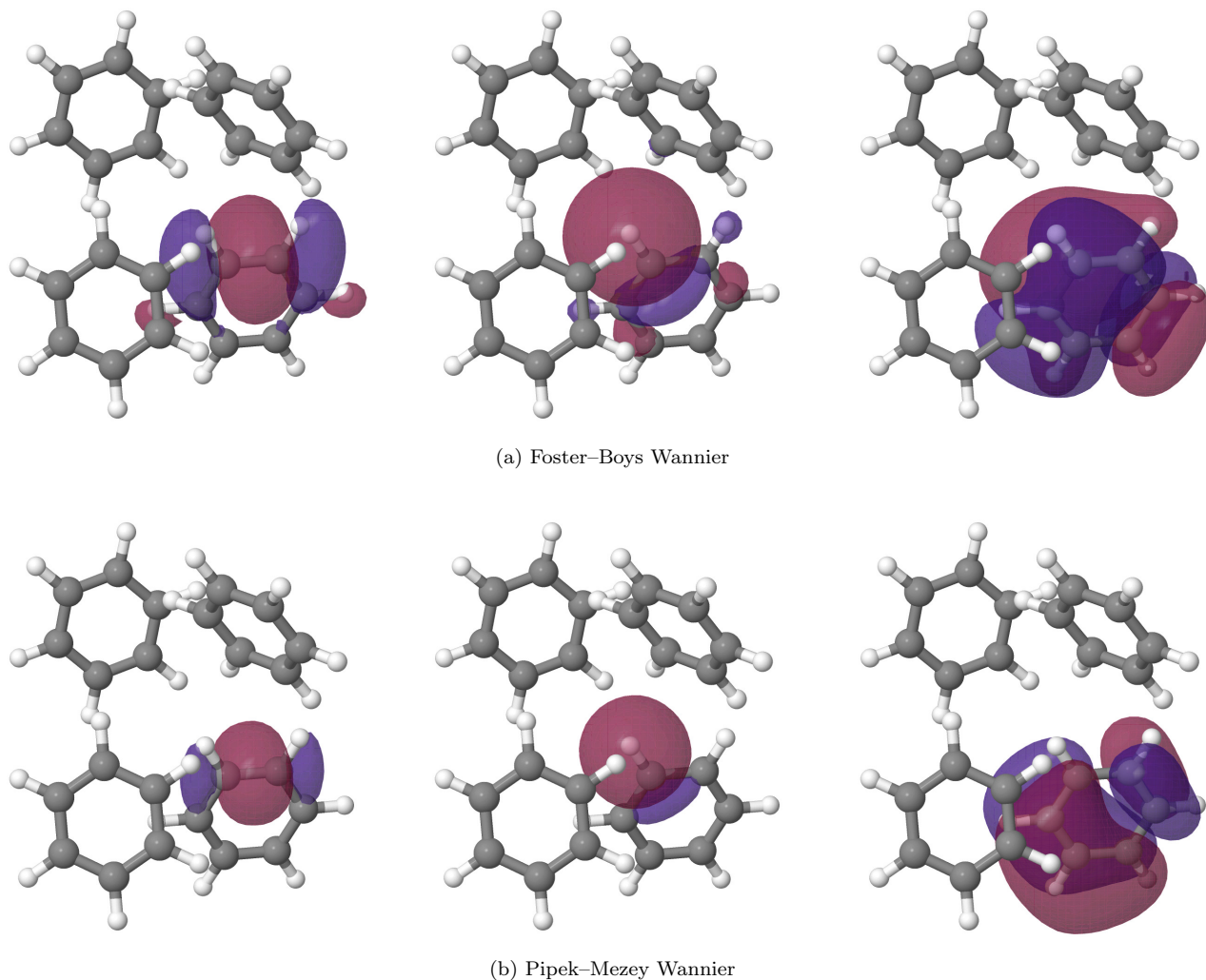


FIG. 5: Foster-Boys function (top row) and Pipek-Mezey Wannier function (bottom row) orbitals of the benzene crystal, represented by four benzene molecules in a three-dimensional periodic lattice (see main text).

“maximally localized Wannier functions”.

PMWFs are just as highly localized as the FBWFs, as revealed by cross-comparison of the values of the objective functions of one of the measures evaluated with the orbitals from the other. The PMWFs do, however, offer an advantage over FBWFs in that a clear separation is obtained between σ - and π -bond orbitals. In the majority of the systems studied here, some of the FBWFs turned out to be a mix of σ and π orbitals resulting in a less clear chemical interpretation. The PMWF method gives localized orbitals that are consistent with chemical intuition in the number of single, double, and triple bonds for carbon and hydrocarbon systems.

Recently, Pipek-Mezey orbitals have been used in molecular calculations, e.g., in studying hydrogen transfer in aryloxy radicals⁵⁸, ring currents in aromatic molecules⁵⁹, hydrogenolysis of nickel-methyl bonds⁶⁰, bonding in an amino-borane rhodium complex⁶¹, as well as electron flow in reaction mechanisms⁶². The introduc-

tion of the PMWF method for condensed matter simulations using periodic boundary conditions opens up new possibilities for the chemical interpretation of, e.g., surface chemistry, where the mixing of σ and π states in the FBWF approach may cause problems for the interpretation of which orbitals of the surface are participating in the reaction, as σ and π electrons typically react in a different way⁶². Thus, we expect the procedure outline here to become widely used in a variety of applications, including theoretical studies of heterogeneous catalysis.

In addition to their use for visualization and interpretation purposes, PMWFs can also be useful for local post-HF methods⁶³. While a FBWF implementation of local Møller-Plesset perturbation theory⁶⁴ truncated at the second order (MP2) has been reported⁶⁵, an implementation based on PMWFs can be expected to have better performance, just as the PM approach has been found to be superior to FB for local treatment of electron correlation effects in molecules⁶⁶.

TABLE V: Localization of the KS-DFT COs (KS), FBWFs and PMWFs as measured by the objective function value of eq (23).

System [†]	$\mathcal{L}(\text{KS})$	$\mathcal{L}(\text{FBWF})$	$\mathcal{L}(\text{PMWF})$	d (%)
b	12.86	14.42	14.40	0.10
co	37.61	52.38	52.31	0.13
sco	65.27	114.10	113.96	0.12
cc $n = 1$	6.85	15.43	15.39	0.22
cc $n = 2$	6.26	31.58	31.56	0.07
cc $n = 3$	7.56	47.70	47.68	0.02
cc $n = 4$	9.22	63.77	63.76	0.01
c-pa $n = 1$	8.66	19.43	19.41	0.11
c-pa $n = 2$	8.04	38.58	39.57	0.04
c-pa $n = 3$	8.57	59.07	59.05	0.03
c-pa $n = 4$	8.95	79.76	79.76	0.00
ac(2,4) $n = 1$	14.27	34.88	34.83	0.15
ac(2,4) $n = 2$	13.48	71.12	71.08	0.06
ac(2,4) $n = 3$	9.66	107.34	107.31	0.03
ac(2,4) $n = 4$	8.81	143.49	143.46	0.02
ac(3,3) $n = 1$	19.58	50.40	50.30	0.20
ac(3,3) $n = 2$	17.31	102.65	102.53	0.12
ac(3,3) $n = 3$	13.88	154.95	154.85	0.07
ac(3,3) $n = 4$	13.41	207.17	207.10	0.04
ac(4,3) $n = 1$	24.10	65.95	65.80	0.23
ac(4,3) $n = 2$	22.95	134.12	133.93	0.14
ac(4,3) $n = 3$	16.04	202.46	202.28	0.09
ac(4,3) $n = 4$	12.73	265.28	264.73	0.21
bn $n = (1, 1)$	7.38	62.88	62.88	0.00
bn $n = (2, 1)$	12.83	125.74	125.73	0.00
bn $n = (2, 2)$	35.71	246.55	246.53	0.01
gp $n = (1, 1)$	7.39	62.08	62.03	0.08
gp $n = (2, 1)$	5.63	126.06	125.97	0.07
gp $n = (2, 2)$	1.84	249.73	249.53	0.05
bc $n = (1, 1, 1)$	1.78	58.80	57.77	0.05
bc $n = (2, 1, 1)$	3.92	117.22	117.14	0.06
bc $n = (2, 2, 1)$	7.68	231.98	231.78	0.09
bc $n = (2, 2, 2)$	13.52	455.40	454.80	0.13

[†] Abbreviations: benzene (b), coronene (co), supercoronene (sco), carbyne chain (cc), $-\text{[C}_8\text{]}_n-$; cis-polyacetylene chain (c-pa), $-\text{[C}_8\text{H}_8\text{]}_n-$; armchair nanoribbon chain (ac(i, j) – width i and length j), $[\text{C}_{8i}\text{H}_8]_n$; boron nitride sheet (bn), $[\text{B}_{16}\text{N}_{16}]_{n=(x,y)}$; graphene sheet (gp), $[\text{C}_{32}]_{n=(x,y)}$; benzene crystal (bc), $[\text{C}_{24}\text{H}_{24}]_{n=(x,y,z)}$.

ACKNOWLEDGMENTS

Computational resources provided by CSC – IT Center for Science, Ltd. (Espoo, Finland) are gratefully acknowledged. This work was funded by the Academy of Finland through its Centres of Excellence Programme (2012–2017) under Project No. 251748, and through its FiDiPro Programme under Project No. 263294.

TABLE VI: Charge localization of the KS-DFT COs (KS), FBWFs and PMWFs as measured by the objective function value of eq (20).

System [†]	$\mathcal{P}(\text{KS})$	$\mathcal{P}(\text{FBWF})$	$\mathcal{P}(\text{PMWF})$	d (%)
b	2.01	6.10	6.16	0.82
co	2.64	21.24	21.46	1.01
sco	3.12	45.67	46.50	1.77
cc $n = 1$	1.64	6.66	6.70	0.59
cc $n = 2$	1.57	13.44	13.54	0.71
cc $n = 3$	1.55	20.22	20.37	0.75
cc $n = 4$	1.55	27.02	27.19	0.61
c-pa $n = 1$	1.40	8.49	8.52	0.32
c-pa $n = 2$	1.22	17.16	17.22	0.37
c-pa $n = 3$	1.18	25.65	25.91	1.03
c-pa $n = 4$	1.25	34.47	34.60	0.36
ac(2,4) $n = 1$	1.35	14.06	14.20	1.01
ac(2,4) $n = 2$	1.11	28.38	28.67	1.03
ac(2,4) $n = 3$	1.12	42.70	43.14	1.03
ac(2,4) $n = 4$	1.05	57.11	57.60	0.84
ac(3,3) $n = 1$	1.49	19.82	20.19	1.88
ac(3,3) $n = 2$	1.21	40.00	40.72	1.77
ac(3,3) $n = 3$	1.11	60.24	61.26	1.67
ac(3,3) $n = 4$	1.08	80.59	81.67	1.46
ac(4,3) $n = 1$	1.57	25.79	26.25	1.72
ac(4,3) $n = 2$	1.24	51.90	52.86	1.82
ac(4,3) $n = 3$	1.14	78.25	79.49	1.57
ac(4,3) $n = 4$	1.09	103.78	105.24	1.39
bn $n = (1, 1)$	1.25	30.44	30.55	0.35
bn $n = (2, 1)$	1.17	61.05	61.44	0.64
bn $n = (2, 2)$	0.97	122.31	123.70	1.13
gp $n = (1, 1)$	0.87	24.07	24.11	0.19
gp $n = (2, 1)$	0.81	48.34	48.50	0.32
gp $n = (2, 2)$	0.68	101.21	101.75	0.54
bc $n = (1, 1, 1)$	2.30	23.89	24.14	1.04
bc $n = (2, 1, 1)$	2.36	48.39	48.86	0.96
bc $n = (2, 2, 1)$	2.81	96.24	97.18	0.96
bc $n = (2, 2, 2)$	3.13	185.94	187.70	0.94

[†] See table V for abbreviations.

VII. APPENDIX

The extension of the generalized overlap matrices under periodic boundary conditions from the Γ -point to \mathbf{k} -point sampling is described in this appendix. Given a unit cell with basis vectors \mathbf{a}_1 , \mathbf{a}_2 and \mathbf{a}_3 , the reciprocal lattice vectors \mathbf{b}_1 , \mathbf{b}_2 and \mathbf{b}_3 are defined. Assuming a uniform sampling of the first Brillouin zone, any \mathbf{k} -point can be expressed as

$$\mathbf{k} = \frac{n_1}{N_1} \mathbf{b}_1 + \frac{n_2}{N_2} \mathbf{b}_2 + \frac{n_3}{N_3} \mathbf{b}_3 \quad (37)$$

TABLE VII: Number of iterations required to converge the PMWF objective function eq (20), $n_{\text{iter.}}^{\text{PMWF}}$, and the FBWF objective function eq (23), $n_{\text{iter.}}^{\text{FBWF}}$. The number of iterations are averaged over fifty independent runs starting with randomly initialized guesses for the rotation matrices \mathbf{W} .

System [†]	$n_{\text{iter.}}^{\text{PMWF}}$	$n_{\text{iter.}}^{\text{FBWF}}$
b	49	83
co	81	107
sco	94	295
cc $n = 1$	686	1398
cc $n = 2$	799	3509
cc $n = 3$	786	4321
cc $n = 4$	733	4177
c-pa $n = 1$	722	682
c-pa $n = 2$	885	1659
c-pa $n = 3$	937	2753
c-pa $n = 4$	925	2609
ac(2,4) $n = 1$	169	817
ac(2,4) $n = 2$	253	2283
ac(2,4) $n = 3$	285	3475
ac(2,4) $n = 4$	314	4177
ac(3,3) $n = 1$	101	1069
ac(3,3) $n = 2$	180	2913
ac(3,3) $n = 3$	272	4377
ac(3,3) $n = 4$	355	4511
ac(4,3) $n = 1$	125	1160
ac(4,3) $n = 2$	184	2690
ac(4,3) $n = 3$	216	4269
ac(4,3) $n = 4$	298	4672
bn $n = (1, 1)$	183	2067
bn $n = (2, 1)$	223	3322
bn $n = (2, 2)$	281	4183
gp $n = (1, 1)$	123	1208
gp $n = (2, 1)$	179	2702
gp $n = (2, 2)$	214	3411
bc $n = (1, 1, 1)$	610	1491
bc $n = (2, 1, 1)$	754	3117
bc $n = (2, 2, 1)$	819	3892
bc $n = (2, 2, 2)$	769	4018

[†] See table V for abbreviations.

where N_i is the number of \mathbf{k} -points in the direction of \mathbf{b}_i , and $n_i = 0, \dots, N_i - 1$. The Bloch states $\psi_{n\mathbf{k}}$ correspond to the Γ -point eigenstates of the repeated cell defined by the extended basis vectors $N_i \mathbf{a}_i$. The reciprocal lattice vectors, \mathbf{G}_α and corresponding weights, g_α , in eqs (20) and (22), now refer to the extended basis vector defined by $N_1 \mathbf{a}_1, N_2 \mathbf{a}_2, N_3 \mathbf{a}_3$.

The weights associated with the objective function val-

ues of eq (20) and eq (23) are normalized such that

$$g_\alpha = \frac{g'_\alpha}{\sum_{\alpha}^{N_\alpha} g'_\alpha} \quad (38)$$

With this definition of weights the objective function values of eq (4) and eq (20) are in agreement between calculations employing open boundaries and those with periodic boundaries (say for a molecule in vacuum). Furthermore, the PMWF and FBWF objective function values, eq (20) and eq (23), respectively, also become systematic with system size.

In the PAW approach⁵⁰ the all-electron (AE) wave functions (WFs) ψ_s are represented in terms of smooth pseudo (PS) waves $\tilde{\psi}_s(\mathbf{r})$

$$\psi_s(\mathbf{r}) = \tilde{\mathcal{T}} \tilde{\psi}_s(\mathbf{r}). \quad (39)$$

The transformation operator $\tilde{\mathcal{T}}$ is given by

$$\tilde{\mathcal{T}} = 1 + \sum_{\mathcal{A}} \sum_i \left(\phi_i^{\mathcal{A}}(\mathbf{r}) - \tilde{\phi}_i^{\mathcal{A}}(\mathbf{r}) \right) \langle \tilde{p}_i^{\mathcal{A}} | \quad (40)$$

where $\phi_i^{\mathcal{A}}$ and $\tilde{\phi}_i^{\mathcal{A}}$ are AE and PS (smooth) partial waves. The partial waves are equal outside atom-centered augmentation spheres of radii $r_c^{\mathcal{A}}$

$$\phi_i^{\mathcal{A}}(\mathbf{r}) = \tilde{\phi}_i^{\mathcal{A}}(\mathbf{r}), \quad |\mathbf{r} - \mathbf{R}^{\mathcal{A}}| > r_c^{\mathcal{A}} \quad (41)$$

where $\mathbf{R}^{\mathcal{A}}$ is the position of atom \mathcal{A} . $\tilde{p}_i^{\mathcal{A}}$ are projector functions, which determine the expansion coefficients of the PS WFs inside the augmentation region. The projector functions are atom centered

$$\tilde{p}_i^{\mathcal{A}}(\mathbf{r}) = \tilde{p}_{n_i l_i}^{\mathcal{A}}(|\mathbf{r} - \mathbf{R}^{\mathcal{A}}|) Y_{l_i m_i} \left(\frac{\mathbf{r} - \mathbf{R}^{\mathcal{A}}}{|\mathbf{r} - \mathbf{R}^{\mathcal{A}}|} \right), \quad (42)$$

where Y_{lm} are spherical harmonics.

The AE WFs are given by

$$\psi_s(\mathbf{r}) = \tilde{\psi}_s(\mathbf{r}) + \sum_{\mathcal{A}} \sum_i \left(\phi_i^{\mathcal{A}}(\mathbf{r}) - \tilde{\phi}_i^{\mathcal{A}}(\mathbf{r}) \right) \langle \tilde{p}_i^{\mathcal{A}} | \tilde{\psi}_s \rangle, \quad (43)$$

where the sum over i indicates a sum over the principal quantum numbers n, l, m in the PAW expansion as given in eq (42). However, the representation of eq (43) is rarely used since it requires an extremely fine grid to properly describe the AE partial wave due to rapid oscillations of $\phi_i^{\mathcal{A}}(\mathbf{r})$ close to $\mathbf{R}^{\mathcal{A}}$.

Instead, within the PAW approach, the expectation value of an operator A , $\langle A \rangle = \sum_s f_s \langle \psi_s | A | \psi_s \rangle$ is expressed in terms of the PS states and a corresponding PS operator \tilde{A} : $\langle A \rangle = \sum_s f_s \langle \tilde{\psi}_s | \tilde{A} | \tilde{\psi}_s \rangle$. A quasilocal operator, such as the real-space projection operator $|\mathbf{r}\rangle \langle \mathbf{r}|$, acting on the PS states has the following form

$$\begin{aligned} \tilde{A} &= \tilde{\mathcal{T}}^\dagger A \tilde{\mathcal{T}} \\ &= A + \sum_{\mathcal{A}} \sum_{i_1 i_2} |\tilde{p}_{i_1}^{\mathcal{A}}\rangle \left(\langle \phi_{i_1}^{\mathcal{A}} | A | \phi_{i_2}^{\mathcal{A}} \rangle - \langle \tilde{\phi}_{i_1}^{\mathcal{A}} | A | \tilde{\phi}_{i_2}^{\mathcal{A}} \rangle \right) \langle \tilde{p}_{i_2}^{\mathcal{A}}|. \end{aligned} \quad (44)$$

The overlap operator $S_{ij} = \langle i|j \rangle$ is

$$\hat{S} = \tilde{\mathcal{T}}^\dagger \tilde{\mathcal{T}} = 1 + \sum_{\mathcal{A}} \sum_{i_1 i_2} |\tilde{p}_{i_1}^{\mathcal{A}}\rangle \Delta S_{i_1 i_2}^{\mathcal{A}} \langle \tilde{p}_{i_2}^{\mathcal{A}}| \quad (45)$$

where

$$\Delta S_{i_1 i_2}^{\mathcal{A}} = \langle \phi_{i_1}^{\mathcal{A}} | \phi_{i_2}^{\mathcal{A}} \rangle - \langle \tilde{\phi}_{i_1}^{\mathcal{A}} | \tilde{\phi}_{i_2}^{\mathcal{A}} \rangle. \quad (46)$$

The PS WFs are orthonormal

$$\langle \tilde{\psi}_r | \hat{S} | \tilde{\psi}_s \rangle = \delta_{rs} \quad (47)$$

only with respect to the PAW overlap operator given in eq (45). This forms the basis for the following overlap schemes to define the partial charge matrices $Q_{mn}^{\mathcal{A}}$ that are used for the generalized Pipek–Mezey localization method.

Using eqs (44) and (47) and the assumption that the atomic weight function centered on \mathcal{A} has negligible weight in the augmentation region around atom \mathcal{A}' , i.e.

$$w_{\mathcal{A}}(\mathbf{r}) | \mathbf{r} \in \mathcal{A}' = \begin{cases} 1 & \text{if } \mathcal{A} = \mathcal{A}' \\ 0 & \text{if } \mathcal{A} \neq \mathcal{A}' \end{cases} \quad (48)$$

the PS partial charge projection operator, $\hat{S}_w^{\mathcal{A}}$, becomes

$$\begin{aligned} \hat{S}_w^{\mathcal{A}} &= \tilde{\mathcal{T}} w_{\mathcal{A}} \tilde{\mathcal{T}} \\ &= w_{\mathcal{A}} + \sum_{\mathcal{A}' \mathcal{A}''} \sum_{i_1 i_2} |\tilde{p}_{i_1}^{\mathcal{A}'}\rangle \langle \tilde{p}_{i_2}^{\mathcal{A}''}| \\ &\quad \times \left(\langle \phi_{i_1}^{\mathcal{A}'} | w_{\mathcal{A}} | \phi_{i_2}^{\mathcal{A}''} \rangle - \langle \tilde{\phi}_{i_1}^{\mathcal{A}'} | w_{\mathcal{A}} | \tilde{\phi}_{i_2}^{\mathcal{A}''} \rangle \right) \\ &= w_{\mathcal{A}} + \sum_{i_1 i_2} |\tilde{p}_{i_1}^{\mathcal{A}}\rangle \Delta S_{i_1 i_2}^{\mathcal{A}} \langle \tilde{p}_{i_2}^{\mathcal{A}}| \end{aligned} \quad (49)$$

where in the last line the condition of eq (48) is used, and the resulting partial charge matrix is simply

$$Q_{rs}^{\mathcal{A}} = \langle \tilde{\psi}_r | w_{\mathcal{A}} | \tilde{\psi}_s \rangle + \sum_{i_1 i_2} \langle \tilde{\psi}_r | \tilde{p}_{i_1}^{\mathcal{A}} \rangle \Delta S_{i_1 i_2}^{\mathcal{A}} \langle \tilde{p}_{i_2}^{\mathcal{A}} | \tilde{\psi}_s \rangle. \quad (50)$$

The first term on the right hand side is given by

$$\langle \tilde{\psi}_r | w_{\mathcal{A}} | \tilde{\psi}_s \rangle = \int \tilde{\psi}_r^*(\mathbf{r}) w_{\mathcal{A}}(\mathbf{r}) \tilde{\psi}_s(\mathbf{r}) d^3r. \quad (51)$$

In the case of periodic systems the partial charge matrix in the CO basis is

$$\begin{aligned} Q_{\alpha, RS}^{\mathcal{A}} &= \langle \tilde{\psi}_R | e^{-\mathbf{G}_\alpha \cdot \mathbf{r}} w_{\mathcal{A}} | \tilde{\psi}_S \rangle + \sum_{i_1 i_2} \langle \tilde{\psi}_R | \tilde{p}_{i_1}^{\mathcal{A}} \rangle \langle \tilde{p}_{i_2}^{\mathcal{A}} | \tilde{\psi}_S \rangle \\ &\quad \times \left(\langle \phi_{i_1}^{\mathcal{A}} | e^{-\mathbf{G}_\alpha \cdot \mathbf{r}} | \phi_{i_2}^{\mathcal{A}} \rangle - \langle \tilde{\phi}_{i_1}^{\mathcal{A}} | e^{-\mathbf{G}_\alpha \cdot \mathbf{r}} | \tilde{\phi}_{i_2}^{\mathcal{A}} \rangle \right) \end{aligned} \quad (52)$$

Now, assuming the phase of the exponential does not vary significantly over the space where $\tilde{p}_i^{\mathcal{A}}$ is nonzero (this approximation is also used in the Foster–Boys Wannier function PAW analog³⁷, and more generally, with ultra-soft pseudopotentials⁶⁷), the integral in the last term can be estimated by

$$e^{-\mathbf{G}_\alpha \cdot \mathbf{R}^{\mathcal{A}}} \sum_{i_1 i_2} \langle \tilde{\psi}_R | \tilde{p}_{i_1}^{\mathcal{A}} \rangle \Delta S_{i_1 i_2}^{\mathcal{A}} \langle \tilde{p}_{i_2}^{\mathcal{A}} | \tilde{\psi}_S \rangle, \quad (53)$$

where we have used the locality of the atomic PAW projectors (eq (48)). We also note that the weight functions in a cell n satisfy

$$w_{\mathcal{A},n}(\mathbf{r} - \mathbf{R}_n) = w_{\mathcal{A},0}(\mathbf{r}) \quad (54)$$

where 0 indicates the cell at the origin, and \mathbf{R}_n is a Bravais lattice vector.

The numerical stability of the Hirshfeld-type partitioning function, eq (26), using the Gaussian model densities is further enforced by employing a cut-off radius, R_c , such that

$$\bar{n}_{\mathcal{A}}^c(\mathbf{r}) = \begin{cases} \bar{n}_{\mathcal{A}}(\mathbf{r}) & \text{if } |\mathbf{r} - \mathbf{R}^{\mathcal{A}}| \leq R_c \\ 0 & \text{otherwise} \end{cases} \quad (55)$$

and we use $\bar{n}_{\mathcal{A}}^c(\mathbf{r})$ to evaluate eq (26). A constant cut-off of 3.8 Å is applied for all types of atoms. Although the partial atomic charge will change when applying a different cut-off, this parameter is not explored further, based on the experience from ref. 21 and the fact that the different choices for the decay parameters result in similar LOs.

Finally, as the real-space grid used to represent the wave functions (coarse grid in GPAW) is uniform, it can lead to problems when the atoms of the system are also distributed uniformly when the Wigner–Seitz (WS) weight function is constructed. For instance, assume two atoms in the system to be placed on the z axis, and the wave function grid spacing to be Δ . Now, if the interatomic separation R is an even multiple of Δ : $\exists n \in \mathcal{N} : R = 2n\Delta$, then the grid points on the $z = n\Delta$ plane will be at the same distance from both nuclei, which would lead the points to contribute with unit weight to both atomic regions, breaking the condition in eq (14). Hence, the WS weight function is modified to rectify this problem by redistributing the weight evenly to all the atoms that share the point as

$$w_{\mathcal{A}}^{\text{WS}}(\mathbf{r}) = \left[\sum_{\mathcal{A}' : \mathbf{r} \in \mathcal{A}'} 1 \right]^{-1}, \quad (56)$$

after which the sum of weights will be unity, once again satisfying eq (14).

- ¹P. Hohenberg and W. Kohn, Phys. Rev. **136**, B864 (1964).
- ²W. Kohn and L. J. Sham, Phys. Rev. **140**, A1133 (1965).
- ³A. D. Becke, J. Chem. Phys. **140**, 18A301 (2014).
- ⁴A. Jain, Y. Shin, and K. A. Persson, Nat. Rev. Mater. **1**, 15004 (2016).
- ⁵B. Silvi and P. Reinhardt, Curr. Org. Chem. **15**, 3555 (2011).
- P. Vidossich and A. Lledós, Dalt. Trans. **43**, 11145 (2014).
- ⁶J. Foster and S. Boys, Rev. Mod. Phys. **32**, 300 (1960).
- ⁷C. Edmiston and K. Ruedenberg, Rev. Mod. Phys. **35**, 457 (1963).
- ⁸R. S. Mulliken, J. Chem. Phys. **23**, 1833 (1955).
- ⁹J. Pipek and P. G. Mezey, J. Chem. Phys. **90**, 4916 (1989).
- ¹⁰W. von Niessen, J. Chem. Phys. **56**, 4290 (1972).
- ¹¹I.-M. Høyvik, B. Jansik, and P. Jørgensen, J. Chem. Phys. **137**, 224114 (2012).
- ¹²A. E. Reed and F. Weinhold, J. Chem. Phys. **83**, 1736 (1985).
- F. Weinhold, C. R. Landis, and E. D. Glendening, Int. Rev. Phys. Chem. **35**, 399 (2016).
- ¹³I.-M. Høyvik and P. Jørgensen, J. Chem. Phys. **138**, 204104 (2013).
- I.-M. Høyvik, B. Jansik, and P. Jørgensen, J. Comput. Chem. **34**, 1456 (2013).
- I.-M. Høyvik, K. Kristensen, T. Kjærgaard, and P. Jørgensen, Theor. Chem. Acc. **133**, 1417 (2014).
- I.-M. Høyvik and P. Jørgensen, Chem. Rev. **116**, 3306 (2016).
- ¹⁴N. Marzari and D. Vanderbilt, Phys. Rev. B **56**, 12847 (1997).
- ¹⁵N. Marzari, A. A. Mostofi, J. R. Yates, I. Souza, and D. Vanderbilt, Rev. Mod. Phys. **84**, 1419 (2012).
- ¹⁶W. C. Lu, C. Z. Wang, T. L. Chan, K. Ruedenberg, and K. M. Ho, Phys. Rev. B **70**, 041101 (2004).
- T.-L. Chan et al., Phys. Rev. B **76**, 205119 (2007).
- X. Qian et al., Phys. Rev. B **78**, 245112 (2008).
- ¹⁷Y. X. Yao, C. Z. Wang, and K. M. Ho, Phys. Rev. B **81**, 235119 (2010).
- ¹⁸G. Wannier, Phys. Rev. **52**, 191 (1937).
- ¹⁹F. Bloch, Zeitschrift für Phys. **57**, 545 (1929).
- ²⁰G. Berghold, C. J. Mundy, A. H. Romero, J. Hutter, and M. Parrinello, Phys. Rev. B **61**, 10040 (2000).
- ²¹S. Lehtola and H. Jónsson, J. Chem. Theory Comput. **10**, 642 (2014).
- ²²F. L. Hirshfeld, Theor. Chim. Acta **44**, 129 (1977).
- ²³T. C. Lillestolen and R. J. Wheatley, Chem. Commun. (Camb). **7345**, 5909 (2008).
- ²⁴T. C. Lillestolen and R. J. Wheatley, J. Chem. Phys. **131**, 144101 (2009).
- ²⁵R. F. W. Bader, *Atoms in Molecules - A Quantum Theory*, Oxford University Press, Oxford, 1990.
- ²⁶J. Cioslowski, J. Math. Chem. **8**, 169 (1991).
- ²⁷D. R. Alcoba, L. Lain, A. Torre, and R. C. Bochicchio, J. Comput. Chem. **27**, 596 (2006).
- ²⁸G. Knizia, J. Chem. Theory Comput. **9**, 4834 (2013).
- ²⁹G. Henkelman, A. Arnaldsson, and H. Jónsson, Comput. Mater. Sci. **36**, 354 (2006).
- E. Sanville, S. D. Kenny, R. Smith, and G. Henkelman, J. Comput. Chem. **28**, 899 (2007).
- W. Tang, E. Sanville, and G. Henkelman, J. Phys. Condens. Matter **21**, 084204 (2009).
- M. Yu and D. R. Trinkle, J. Chem. Phys. **134**, 064111 (2011).
- ³⁰P. Bultinck, C. Van Alsenoy, P. W. Ayers, and R. Carbó-Dorca, J. Chem. Phys. **126**, 144111 (2007).
- ³¹D. E. P. Vanpoucke, P. Bultinck, and I. Van Driessche, J. Comput. Chem. **34**, 405 (2013).
- C. M. Zicovich-Wilson, M. Hó, A. M. Navarrete-López, and S. Casassa, Theor. Chem. Acc. **135**, 188 (2016).
- ³²S. Lehtola and H. Jónsson, J. Chem. Theory Comput. **9**, 5365 (2013).
- ³³S. Lehtola and H. Jónsson, J. Chem. Theory Comput. **10**, 5324 (2014).
- ³⁴S. Lehtola, M. Head-Gordon, and H. Jónsson, J. Chem. Theory Comput. **12**, 3195 (2016).
- ³⁵A. Heßelmann, J. Chem. Theory Comput. **12**, 2720 (2016).
- ³⁶K. S. Thygesen, L. B. Hansen, and K. W. Jacobsen, Phys. Rev. Lett. **94**, 026405 (2005).
- ³⁷K. S. Thygesen, L. B. Hansen, and K. W. Jacobsen, Phys. Rev. B **72**, 125119 (2005).
- ³⁸R. Sakuma, Phys. Rev. B - Condens. Matter Mater. Phys. **87**, 1 (2013).
- ³⁹R. Resta and S. Sorella, Phys. Rev. Lett. **82**, 370 (1999).
- ⁴⁰P. L. Silvestrelli, Phys. Rev. B **59**, 9703 (1999).
- ⁴¹P. L. Silvestrelli, N. Marzari, D. Vanderbilt, and M. Parrinello, Solid State Commun. **107**, 7 (1998).
- ⁴²S. F. Boys, Localized Orbitals and Localized Adjustment Functions, in *Quantum theory atoms, Mol. solid state a Tribut. to John C. Slater*, edited by P.-O. Löwdin, Academic Press, New York, 1966.
- ⁴³I. Souza, N. Marzari, and D. Vanderbilt, Phys. Rev. B **65**, 035109 (2001).
- ⁴⁴P. Bultinck, P. W. Ayers, S. Fias, K. Tiels, and C. Van Alsenoy, Chem. Phys. Lett. **444**, 205 (2007).
- ⁴⁵T. Verstraelen, P. W. Ayers, V. Van Speybroeck, and M. Waroquier, J. Chem. Theory Comput. **9**, 2221 (2013).
- ⁴⁶H. Oberhofer and J. Blumberger, J. Chem. Phys. **131**, 064101 (2009).
- ⁴⁷J. J. Mortensen, L. B. Hansen, and K. W. Jacobsen, Phys. Rev. B **71**, 035109 (2005).
- J. Enkovaara et al., J. Phys. Condens. Matter **22**, 253202 (2010).
- ⁴⁸A. H. Larsen, M. Vanin, J. J. Mortensen, K. S. Thygesen, and K. W. Jacobsen, Phys. Rev. B **80**, 195112 (2009).
- ⁴⁹J. P. Perdew, K. Burke, and M. Ernzerhof, Phys. Rev. Lett. **77**, 3865 (1996).
- J. P. Perdew, K. Burke, and M. Ernzerhof, Phys. Rev. Lett. **78**, 1396 (1997).
- ⁵⁰P. E. Blöchl, Phys. Rev. B **50**, 17953 (1994).
- ⁵¹H. J. Monkhorst and J. D. Pack, Phys. Rev. B **13**, 5188 (1976).
- ⁵²S. R. Bahn and K. W. Jacobsen, Comput. Sci. Eng. **4**, 56 (2002).
- ⁵³X. Gonze et al., Comput. Mater. Sci. **25**, 478 (2002).
- X. Gonze et al., Comput. Phys. Commun. **180**, 2582 (2009).
- ⁵⁴M. Valiev et al., Comput. Phys. Commun. **181**, 1477 (2010).
- ⁵⁵G. Kresse and J. Furthmüller, Phys. Rev. B **54**, 11169 (1996).
- G. Kresse and D. Joubert, Phys. Rev. B **59**, 1758 (1999).
- ⁵⁶Jmol: an open-source Java viewer for chemical structures in 3D. <http://www.jmol.org>.
- ⁵⁷F. Aquilante, T. B. Pedersen, A. Sánchez de Merás, and H. Koch, J. Chem. Phys. **125**, 174101 (2006).
- ⁵⁸Y.-Z. Chen, Y.-H. Tian, M. Kertesz, and R. G. Weiss, Photochem. Photobiol. Sci. **9**, 1203 (2010).
- ⁵⁹C. M. Gibson and P. W. Fowler, Tetrahedron Lett. **55**, 2078 (2014).
- ⁶⁰N. Curado, C. Maya, J. López-Serrano, and A. Rodríguez, Chem. Commun. **50**, 15718 (2014).
- ⁶¹A. Kumar, N. A. Beattie, S. D. Pike, S. A. Macgregor, and A. S. Weller, Angew. Chemie Int. Ed. **55**, 6651 (2016).
- ⁶²G. Knizia and J. E. M. N. Klein, Angew. Chemie Int. Ed. **54**, 5518 (2015).
- ⁶³P. Pulay, Chem. Phys. Lett. **100**, 151 (1983).
- S. Saebø and P. Pulay, Annu. Rev. Phys. Chem. **44**, 213 (1993).
- ⁶⁴C. Møller and M. S. M. Plesset, Phys. Rev. **46**, 618 (1934).
- ⁶⁵S. Casassa, C. M. Zicovich-Wilson, and C. Pisani, Theor. Chem. Acc. **116**, 726 (2006).
- C. Pisani et al., J. Comput. Chem. **29**, 2113 (2008).
- ⁶⁶J. W. Boughton and P. Pulay, J. Comput. Chem. **14**, 736 (1993).
- ⁶⁷L. Bernasconi and P. Madden, J. Mol. Struct. THEOCHEM **544**, 49 (2001).